

Exploring the multi-band emission of TXS 0536+145: the most distant γ -ray flaring blazar

M. Orienti^{1*}, F. D’Ammando^{1,2}, M. Giroletti¹, J. Finke³, M. Ajello⁴,
D. Dallacasa^{1,2}, T. Venturi¹

¹*INAF – Istituto di Radioastronomia, via Gobetti 101, I-40129, Bologna, Italy*

²*Dipartimento di Fisica e Astronomia, Università degli Studi di Bologna, via Ranzani 1, I-40127 Bologna, Italy*

³*US Naval Research Laboratory, Code 7653, Washington, DC, USA*

⁴*Department of Physics and Astronomy, Clemson University, Clemson, SC 29634, USA*

Received 8 March 2022; accepted ?

ABSTRACT

We report results of a multi-band monitoring campaign of the flat spectrum radio quasar TXS 0536+145 at redshift 2.69. This source was detected during a very high γ -ray activity state in 2012 March by the Large Area Telescope on board *Fermi*, becoming the γ -ray flaring blazar at the highest redshift detected so far. At the peak of the flare the source reached an apparent isotropic γ -ray luminosity of 6.6×10^{49} erg s⁻¹ which is comparable to the values achieved by the most luminous blazars. This activity triggered radio-to-X-rays monitoring observations by *Swift*, Very Long Baseline Array, European VLBI Network, and Medicina single-dish telescope. Significant variability was observed from radio to X-rays supporting the identification of the γ -ray source with TXS 0536+145. Both the radio and γ -ray light curves show a similar behaviour, with the γ -rays leading the radio variability with a time lag of about 4–6 months. The luminosity increase is associated with a flattening of the radio spectrum. No new superluminal component associated with the flare was detected in high resolution parsec-scale radio images. During the flare the γ -ray spectrum seems to deviate from a power law, showing a curvature that was not present during the average activity state. The γ -ray properties of TXS 0536+145 are consistent with those shown by the high-redshift γ -ray blazar population.

Key words: radiation mechanisms: non-thermal - gamma-rays: general - radio continuum: general - galaxies quasars: individual (TXS 0536+145)

1 INTRODUCTION

High-redshift blazars are among the most powerful objects in the Universe. Although they represent a significant fraction (~ 22 per cent) of the extragalactic hard X-ray sources (e.g. Ajello et al. 2012), they are not commonly detected in γ -rays. Only 35 out of 360 flat spectrum radio quasars (FSRQ) detected by the Large Area Telescope (LAT) on board *Fermi* and listed in the Second LAT Catalogue of Active Galactic Nuclei (2LAC) have redshift $z > 2$ (Ackermann et al. 2011). In the first LAT catalogue of γ -ray sources above 10 GeV (1FHL) only 7 sources with $z > 2$ are detected (Ackermann et al. 2013). They are FSRQ already listed in the 2LAC sample, and represent the 20 per cent of the FSRQ with $z > 2$ present in the 2LAC.

Despite their low fraction in high-energy catalogues, the γ -ray emission from high-redshift blazars is a powerful tool for probing the extragalactic background light (EBL). This diffuse radiation consists of photons likely produced by stars and galaxies across the Universe and its lifetime. As the high-energy photons from extragalactic sources propagate through the Universe, they interact with EBL photons at ultraviolet through optical wavelengths by γ - γ absorption, and create electron-positron pairs (e.g. Gould & Schreder 1967). This results in an attenuation of the γ -ray sources above a critical energy that depends on the redshift and the EBL model assumed (e.g. Franceschini et al. 2008).

So far, no absorption feature related to the EBL has been unambiguously observed in the spectra of individual sources. The EBL attenuation has been also investigated by combining the spectra of a sample of γ -ray BL Lacs detected above 3 GeV and spanning a redshift range between 0.03 and 1.6 (Ackermann et al. 2012). For local sources ($z < 0.2$), no

* E-mail: orienti@ira.inaf.it

EBL attenuation is observed up to 120 GeV. The absorption feature is clearly visible for sources with $z > 0.2$, and evolves with redshift. The lack of BL Lacs above $z > 1.6$ precluded a statistical approach for investigating the EBL attenuation at higher redshifts. This information can be obtained by the analysis of the spectra of FSRQ, whose high redshift distribution extends beyond $z = 2.5$. The analysis of the FSRQ detected above 10 GeV suggested that sources become softer with increasing redshift. This is particularly evident for the FSRQ from the 1FHL with $z > 2$. The spectral softening above 10 GeV (and not above 100 MeV) is interpreted as evidence of EBL attenuation, although a cosmological evolution of the photon index cannot be ruled out (Ackermann et al. 2012).

The detection of FSRQ at $z > 2$ during γ -ray flaring activity may provide a step forward in our understanding of the EBL attenuation. During γ -ray flaring episodes the spectra of FSRQ show a moderate hardening (Abdo et al. 2010a), allowing us to explore energies that are usually strongly attenuated due to the intrinsic source spectrum. So far, 10 blazars at $z > 2$ have been detected during γ -ray flaring activity. One of these objects is TXS 0536+145, which was detected during a γ -ray flare on 2012 March 22 by *Fermi*-LAT (Orienti & D’Ammando 2012). With a redshift of $z = 2.69$ (Sowards-Emmerd et al. 2005), this source is the γ -ray flaring blazar at the highest redshift observed so far.

TXS 0536+145 was not part of the 1FGL or 2FGL catalogues (Abdo et al. 2010b; Nolan et al. 2012), indicating its low activity state during the first two years of *Fermi*-LAT observations. The high-energy flare triggered a multi-wavelength monitoring campaign in X-rays, optical (*Swift*, XRT and UVOT) and radio bands (Very Long Baseline Array (VLBA), European VLBI Network (EVN) interferometers, and Medicina single-dish telescope). In this paper we present the results of the multi-band campaign. In particular we investigate the possible connection between the γ -ray flare and flux variability in low-energy bands, as well as changes in the radio jet structure. The information is then used to determine the physical properties of this extreme object and to model its spectral energy distribution (SED) during the flaring state.

The paper is organized as follows. In Section 2 we present the *Fermi*-LAT data analysis and results. In Section 3 we report the radio data collected by VLBA, EVN, and the Medicina single-dish telescope, while in Section 4 we present the *Swift* observations performed in 2012 April and November. Results of the multi-wavelength campaign are presented in Section 5. The discussion and the presentation of the SED modelling is given in Section 6, while a brief summary is in Section 7.

Throughout this paper, we assume the following cosmology: $H_0 = 71 \text{ km s}^{-1} \text{ Mpc}^{-1}$, $\Omega_M = 0.27$ and $\Omega_\Lambda = 0.73$, in a flat Universe. At the redshift of the target, $z = 2.69$ (Sowards-Emmerd et al. 2005), the luminosity distance D_L is 22600 Mpc, and 1 milliarcsecond = 8.06 pc.

2 FERMI-LAT DATA: SELECTION AND ANALYSIS

The *Fermi*-LAT is a pair-conversion telescope operating from 20 MeV to > 300 GeV. It has a large peak effective

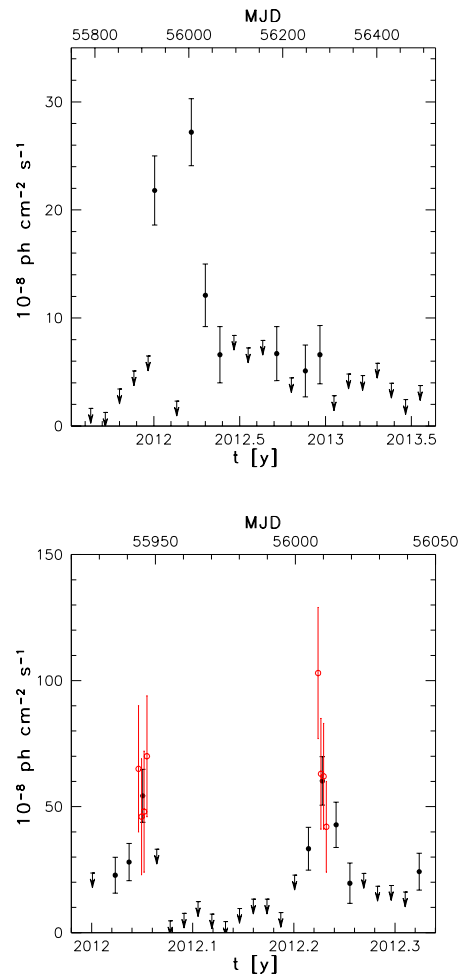


Figure 1. *Top:* Integrated LAT light curve of TXS 0536+145 obtained in the 0.1–100 GeV energy range during 2011 August 4 – 2013 August 4 with 1-month time bins. Arrows refer to $2\text{-}\sigma$ upper limits on the source flux. Upper limits are computed when $\text{TS} < 10$. *Bottom:* Integrated LAT light curve of TXS 0536+145 obtained in the 0.1–100 GeV energy range during 2012 January 1 – 2012 April 30 with 5-day time bins. Open circles refer to daily flux for the high activity periods. Arrows refer to $2\text{-}\sigma$ upper limits on the source flux. Upper limits are computed when $\text{TS} < 10$.

area ($\sim 8000 \text{ cm}^2$ for 1 GeV photons), an energy resolution of typically ~ 10 per cent, and a field of view of about 2.4 sr with single-photon angular resolution (radius of 68 per cent containment angle) of 0.6° at $E = 1$ GeV on-axis. Details of the *Fermi*-LAT are given in Atwood et al. (2009).

The LAT data reported in this paper were collected from 2008 August 4 (MJD 54682) to 2013 August 4 (MJD 56508). During this time the LAT instrument operated almost entirely in survey mode. The analysis was performed with the *ScienceTools*¹ software package version v9r32p5. Only events belonging to the “Source” class were

¹ <http://fermi.gsfc.nasa.gov/ssc/data/analysis/>

selected. In addition, a cut on the zenith angle ($< 100^\circ$) was applied to reduce contamination from the Earth limb γ -rays, which are produced by cosmic rays interacting with the upper atmosphere. Moreover, only photons detected when the spacecraft rocking angle was $< 52^\circ$ were selected. The spectral analysis was performed with the instrument response functions P7REP_SOURCE_V15 using the unbinned maximum likelihood method implemented in the tool `gtlike`. A Galactic diffuse emission model and the isotropic component, which is the sum of an extragalactic and residual cosmic-ray background, were used to model the background². The normalizations of both components in the background model were allowed to vary freely during the spectral fitting.

We analysed a region of interest of 10° radius centred at the location of TXS 0536+145. We evaluated the significance of the γ -ray signal from the sources by means of the maximum likelihood Test Statistic $TS = 2\Delta\log(\text{likelihood})$ between models with and without a point source at the position of TXS 0536+145 (Mattox et al. 1996). The source model used in `gtlike` includes all the point sources from the 2FGL catalogue and from the preliminary list of the Third Fermi LAT Catalogue (Ackermann et al., in preparation) that fall within 15° from TXS 0536+145. The spectra of these sources were parametrized by power-law functions, $dN/dE \propto (E/E_0)^{-\Gamma_\gamma}$, or log-parabola, $dN/dE \propto E/E_0^{-\alpha-\beta \log(E/E_0)}$, as reported in the 2FGL catalogue for the different sources (Nolan et al. 2012). In the same way a power law with super-exponential cut-off has been used for the bright pulsars in the field. A first maximum likelihood analysis was performed to remove from the model the sources having $TS < 10$ and/or a predicted number of counts based on the fitted model $N_{pred} < 3$. A second maximum likelihood analysis was performed on the updated source model. The fitting procedure was performed with the sources within 10° from TXS 0536+145 included with the normalization factors and the photon indices left as free parameters. For the sources located between 10° and 15° from our target we kept the normalization and the photon index fixed to the values of the 2FGL catalogue.

Integrating over the first two years of *Fermi* operation the fit yielded a $TS = 2$, with a $2\text{-}\sigma$ upper limit of 1.0×10^{-8} ph $\text{cm}^{-2} \text{s}^{-1}$ in the 0.1–100 GeV energy range and assuming $\Gamma_\gamma = 2.37$. In the same way integrating in the period 2010 August 4 – 2011 August 4 (MJD 55412–55777) the fit yielded a $TS = 2$, with a $2\text{-}\sigma$ upper limit of 4.5×10^{-9} ph $\text{cm}^{-2} \text{s}^{-1}$ in the 0.1–100 GeV energy range. By contrast, the fit with a power-law model to the data integrated over the fourth and fifth years of *Fermi* operation (2011 August 4 – 2013 August 4; MJD 55777–56508) in the 0.1–100 GeV energy range results in a $TS = 142$, with an integrated average flux of $(4.2 \pm 0.6) \times 10^{-8}$ ph $\text{cm}^{-2} \text{s}^{-1}$ and a photon index $\Gamma_\gamma = 2.37 \pm 0.09$. The upper panel of Fig. 1 shows the γ -ray light curve for the period 2011 August 4 – 2013 August 4 using a power-law model and 1-month time bins. For each time bin the spectral parameters of TXS 0536+145 and all sources within 10° from the target were frozen to the value resulting from the likelihood analysis over the entire period. If $TS < 10$ the value of the

fluxes were replaced by the $2\text{-}\sigma$ upper limits.

On a monthly time scale the source was detected for the first time in 2012 January, with an increasing activity in 2012 March followed by a lower flux in 2012 April–May. After this period the source was detected at a low flux level only in 2012 September, November, and December.

Leaving the photon index free to vary during the month of the highest activity (2012 March 4 – April 4) the fit results in a photon index $\Gamma_\gamma = 2.05 \pm 0.08$ and a $TS=183$.

We produced a light curve focused on the period of high activity (2012 January – April) with 5-day and 1-day time bins (Fig. 1, bottom panel). We used a 1-day time bin for the period with higher statistics. A preliminary measurement of the peak flux on 22 March was reported by Orienti & D’Ammando (2012). The daily averaged flux in the detailed analysis was $(1.0 \pm 0.3) \times 10^{-6}$ ph $\text{cm}^{-2} \text{s}^{-1}$, a factor of ~ 25 higher than the average flux estimated considering together the fourth and fifth years of *Fermi*-LAT observations. The corresponding observed apparent isotropic γ -ray luminosity peak is 6.6×10^{49} erg s^{-1} in the 0.1–100 GeV energy range, comparable to the values reached by the most powerful FSRQ during flaring activity.

The γ -ray point source localization was determined by the use of the `gtfindsrc` tool applied to the γ rays extracted over the period 2011 August 4 – 2013 August 4, and results in R.A. = 84:908, Dec. = 14:604 (J2000), with a 95% error circle radius of $0:07$, at an angular separation of $0:05$ from the radio position of TXS 0536+145. This likely indicates a physical association between the γ -ray source and the low-energy counterpart.

In order to investigate the presence of a curvature in the γ -ray spectrum of TXS 0536+145 an alternative spectral model to the power law (PL), a log parabola (LP) was used for the fit. By analysing the fourth and fifth years of *Fermi*-LAT observations we obtained a spectral slope $\alpha = 2.05 \pm 0.09$ at the reference energy $E_0 = 300$ MeV, a curvature parameter around the peak $\beta = 0.11 \pm 0.07$, with a $TS = 142$ and an integrated average flux of $(3.2 \pm 0.5) \times 10^{-8}$ ph $\text{cm}^{-2} \text{s}^{-1}$ in the 0.1 – 100 GeV energy range. We used a likelihood ratio test to check the PL model (null hypothesis) against the LP model (alternative hypothesis). These values can be compared by defining the curvature Test Statistic $TS_{\text{curve}} = TS_{\text{LP}} - TS_{\text{PL}}$, which we find to be $TS_{\text{curve}} = 0$. Therefore, no statistical evidence of a curved spectral shape is detected.

If we consider only the flaring period (2012 March), using a log-parabola model we obtain a spectral slope $\alpha = 1.52 \pm 0.13$ at the reference energy $E_0 = 300$ MeV, a curvature parameter around the peak $\beta = 0.16 \pm 0.04$, with a $TS = 202$. In this case we have $TS_{\text{curve}} = TS_{\text{LP}} - TS_{\text{PL}} = 19$ corresponding to $\sim 4.4\text{-}\sigma$, indicating statistical evidence of a curved spectral shape. By means of the `gtsrcprob` tool we estimated that the highest energy photon emitted by TXS 0536+145 (with probability > 80 per cent of being associated with the source) was observed on 2012 March 22 at a distance of $0:05$ from the source with an energy of 11.2 GeV. The highest energy photon was detected at the peak of the γ -ray high activity state.

Analysing the *Fermi*-LAT data with $E > 10$ GeV collected between 2011 August and 2013 August, the fit with a power-law model resulted in a $TS=5$, indicating that the

² <http://fermi.gsfc.nasa.gov/ssc/data/access/lat/BackgroundModels.html>

source was not detected at such high energy. We evaluated the $2\text{-}\sigma$ upper limit as 9.3×10^{-11} ph cm $^{-2}$ s $^{-1}$ (assuming $\Gamma_\gamma = 2.37$).

3 RADIO DATA

3.1 VLBA observations

Multi-frequency Target of Opportunity (ToO) VLBA observations (project code BO042) of TXS 0536+145 triggered by the γ -ray flare were carried out at 8.4, 15, and 24 GHz during five observing epochs between 2012 May and 2013 January, with a recording bandwidth of 16 MHz at 512 Mbps data rate. During each observing epoch, the source was observed for 20 min at 8.4 GHz, and for 40 min at 15 and 24 GHz, spread into several scans of about 4 min each, and cycling through frequencies in order to improve the uv -coverage. For this reason the flux density measurements of the pc-scale emission at the various frequencies can be considered roughly simultaneous during each epoch. The observing epochs are separated by about 2 months.

Data reduction was performed using the NRAO’s Astronomical Image Processing System (AIPS). After the application of system temperature and antenna gain information, the amplitudes were checked using the data on DA 193 (J0555+398) which is unresolved on a large subset of baselines at all frequencies, and whose flux density is monitored at the JVLA³. DA 193 was also used to generate the bandpass correction. The source PKS 0528+134 was used as phase calibrator.

The uncertainties on the amplitude calibration were found to be approximately 7 per cent at 8.4 and 15 GHz, and about 10 per cent at 24 GHz. The target source is strong enough to allow the fringe fitting with a solution interval of one minute to preserve the phase coherence. Final images were produced after a number of phase self-calibration iterations. Amplitude self-calibration was applied using a solution interval longer than the scan length to remove residual systematic errors at the end of the self-calibration process. The $1\text{-}\sigma$ noise level measured on the image plane is about 0.15 - 0.17 mJy/beam, being worse at higher frequency. For a source as bright as our target, the error on the flux density is dominated by the calibration uncertainty. The restoring beam is about 2.2×0.8 mas 2 , 1.4×0.5 mas 2 , and 0.8×0.2 mas 2 at 8.4, 15, and 24 GHz, respectively.

At 15 GHz we complemented our VLBA data with five additional observations from the Monitoring Of Jets in Active galactic nuclei with VLBA Experiments (MOJAVE) programme⁴ (Lister et al. 2009a) performed between 2012 April and 2013 August. Uncertainties on the flux density scale are approximately 5 per cent (Lister et al. 2013). Results on the ToO VLBA and MOJAVE observations are reported in Table 1.

In addition to the ToO observations, we retrieved four epochs of archival VLBA data obtained in 2011 at 8.4 GHz (project code BC196) to study the light curve before the

Table 1. VLBA flux density of TXS 0536+145. Column 1: observing date; Cols. 2, 3, and 4: VLBA flux density at 8.4, 15, and 24 GHz, respectively; Col. 5: spectral index between 8.4 and 15 GHz; Col. 6: spectral index between 15 and 24 GHz.

Obs. date	$S_{8.4}$ mJy	S_{15} mJy	S_{24} mJy	$\alpha_{8.4}^{15}$	α_{15}^{24}
29/04/2012	-	777±39 ^a	-	-	-
22/05/2012	479±33	830±58	926±93	-0.95±0.17	-0.25±0.25
23/07/2012	576±40	661±46	705±70	-0.25±0.17	-0.15±0.25
26/09/2012	686±48	804±56	927±93	-0.30±0.17	-0.30±0.25
19/11/2012	758±53	833±58	785±78	-0.20±0.17	0.10±0.25
21/11/2012	-	805±40 ^a	-	-	-
13/01/2013	761±53	719±50	708±70	0.10±0.17	0.05±0.25
10/02/2013	-	626±31 ^a	-	-	-
02/06/2013	-	498±25 ^a	-	-	-
12/08/2013	-	488±25 ^a	-	-	-

^aMOJAVE data

Table 2. Archival VLBA data at 8.4 GHz of TXS 0536+145. Column 1: observing date; Col. 2: on-source observing time; Col. 3: flux density at 8.4 GHz.

Obs. date	Obs. time min	$S_{8.4}$ mJy
01/02/2011	2.3	275±14
30/05/2011	3.2	260±13
06/08/2011	4.7	280±14
01/09/2011	3.2	200±10

γ -ray flare (see Table 2). The calibration and data reduction were performed in the same way as described above. In these observing runs, TXS 0536+145 was observed for a few minutes as a phase calibrator, precluding an adequate uv -coverage for investigating changes in the radio structure, whereas the data turned out to be useful to measure the pc-scale flux density.

3.2 EVN observations

Target of Opportunity EVN observations at 22 GHz were triggered by the γ -ray flare and carried out between 2012 June and 2013 October, during the standard EVN sessions. The observations were performed using eight sub-bands separated by 16 MHz each for an aggregate bit rate of 1 Gbps. The telescopes involved in the observing runs that provided good data are listed in Table 3. Fig. 2 displays the VLBA and EVN uv -coverages. It is worth noting the lack of baselines shorter than 40 M λ in the EVN uv -coverage that prevents the detection of features larger than ~ 5 mas. On the other hand, the lack of baselines longer than 200 M λ in the North-South direction of the VLBA uv -coverage decreases the resolution along that direction due to the elongated shape of the observing beam.

Data reduction was performed using AIPS. A priori amplitude calibration was derived with the AIPS task APCAL on

³ http://www.aoc.nrao.edu/~smyers/evlapolcal/polcal_master.htm

⁴ The MOJAVE data archive is maintained at <http://www.physics.purdue.edu/MOJAVE>.

Table 3. EVN observations of TXS 0536+145. Column 1: observing date; Col. 2: 22 GHz flux density; Cols. 3 and 4: beam size and beam position angle, respectively; Col. 5: $1\text{-}\sigma$ noise level measured on the image plane; Col. 6: Antennas. Ef=Effelsberg; On=Onsala; Yb=Yebes; Sv=Svetloe; Zc=Zelenchukskaya; Ur=Urumqi; Hh=Hartebeesthoek; Nt=Noto; Sh=Shangai; Md=Medicina; Tr=Torun; Mh=Metsähovi; Bd=Badary.

Obs. date	S_{22} mJy	Beam size mas ²	PA deg	rms mJy/beam	Notes
06/06/2012	646±64	0.65×0.23	0.11	0.5	Ef,On,Yb,Sv,Zc,Ur,Hh
06/11/2012	721±72	1.41×0.17	5.62	0.3	Ef,On,Yb,Nt,Zc,Ur,Sh
27/02/2013	530±53	1.21×0.23	4.11	0.2	Ef,On,Md,Nt,Tr,Yb,Mh,Ur,Sh
11/06/2013	490±49	0.56×0.47	59.17	0.3	Ef,On,Md,Nt,Tr,Yb,Zc,Hh
17/10/2013	421±42	0.53×0.22	-2.64	0.4	Ef,On,Md,Nt,Tr,Yb,Sv,Zc,Bd,Ur,Sh,Hh

Table 4. Medicina observations of TXS 0536+145.

Date	$S_{5\text{GHz}}$ mJy	$S_{8.4\text{GHz}}$ mJy
20/04/2012	275±20	365±15
21/05/2012	-	440±30
02/08/2012	-	470±40
06/09/2012	-	600±40
05/10/2012	550±10	750±50

the basis of the measurements of the system temperatures and the antenna gain information for each antenna. The flux density scale was checked by means of the calibrator PKS 0528+134 which was observed as a calibrator also with the VLBA. The uncertainty on the flux density is approximately 10 per cent. PKS 0528+134 was also used as bandpass calibrator.

TXS 0536+145 is strong enough to allow the fringe fitting with a solution interval of 1 min to preserve the phase coherence. Final images were produced after a number of phase self-calibration iterations.

3.3 Medicina observations

After the 2012 April γ -ray flare, TXS 0536+145 was observed five times with the Medicina single-dish telescope at 5 and 8.4 GHz. Observations were performed with the new Enhanced Single-dish Control System, which provides enhanced sensitivity and supports observations with the cross scan technique. At each frequency the typical on source time is 40 seconds and the flux density was calibrated with respect to 3C 286, 3C 48, and NGC 7027. Since the signal-to-noise ratio in each scan across the source was low (typically 3), we performed a stacking analysis of the scans, which allowed us to significantly improve the signal-to-noise ratio and the accuracy of the measurement. The flux densities at 5 and 8.4 GHz measured with the Medicina telescope are listed in Table 4.

4 SWIFT DATA: ANALYSIS AND RESULTS

The *Swift* satellite (Gehrels et al. 2004) performed three observations of TXS 0536+145 in 2012. The first two were car-

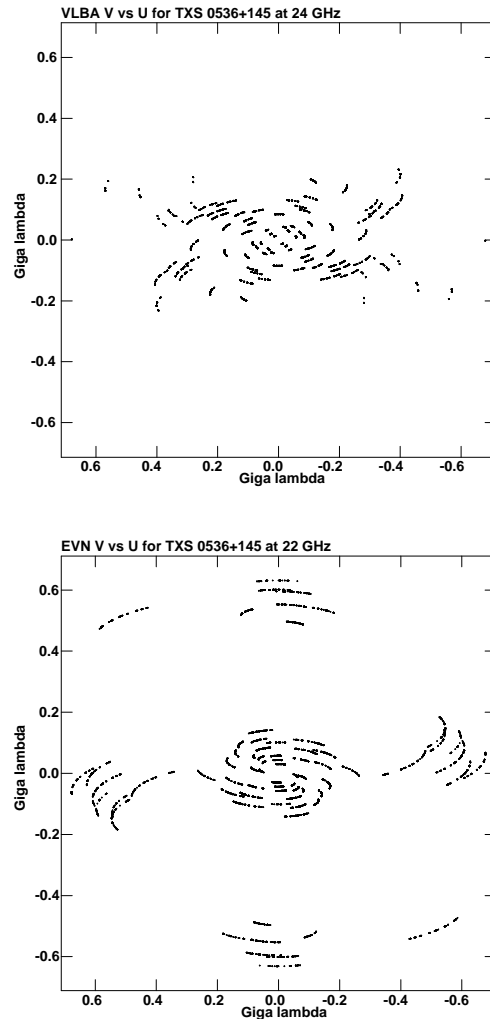


Figure 2. *Top:* VLBA uv -coverage at 24 GHz; *Bottom:* EVN uv -coverage at 22 GHz. The plots represent the uv -coverage of the VLBI network in units of wavelengths.

ried out a few days after the high γ -ray activity detected by *Fermi*-LAT at the end of March. The last observation took place a few months later, to check the flux variability. The observations were performed with all three on board instruments: the X-ray Telescope (XRT; Burrows et al. 2005,

Table 5. Log and fitting results of *Swift*/XRT observations of TXS 0536+145 using a power-law model with N_{H} fixed to Galactic absorption.

Obs. date	Net Exposure Time s	Net Count Rate 10^{-3} cps	Photon index Γ_{X}	Flux 0.3–10 keV ^a 10^{-13} erg cm ⁻² s ⁻¹
04/04/2012	1948	4.3 ± 0.5	1.6 ± 0.3	2.7 ± 0.9
18/04/2012	2630	2.5 ± 0.3	2.0 ± 0.4	1.2 ± 0.3
15/11/2012	3679	2.4 ± 0.3	1.5 ± 0.3	1.4 ± 0.2

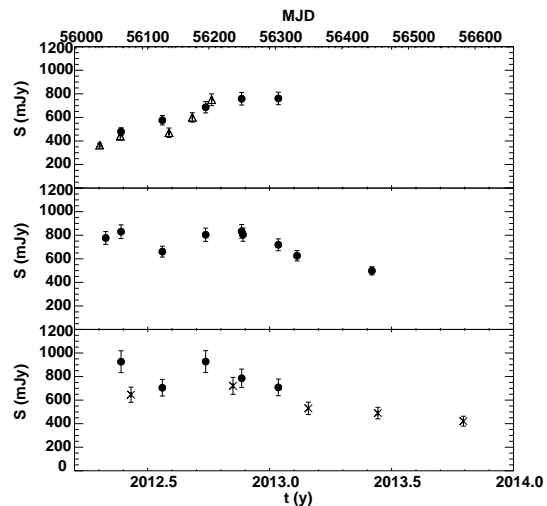
^aObserved flux

0.2–10.0 keV), the Ultraviolet/Optical Telescope (UVOT; Roming et al. 2005, 170–600 nm) and the Burst Alert Telescope (BAT; Barthelmy et al. 2005, 15–150 keV).

The hard X-ray flux of this source turned out to be below the sensitivity of the BAT instrument for such short exposures and therefore the data from this instrument are not used. It is worth mentioning that the source was not present in the *Swift* BAT 70-month hard X-ray catalogue (Baumgartner et al. 2013).

The XRT data were processed with standard procedures (`xrtpipeline v0.12.6`), filtering, and screening criteria by using the `HEASoft` package (v6.12). The data were collected in photon counting mode in all the observations. The source count rate was low (< 0.5 counts s⁻¹); thus pile-up correction was not required. Source events were extracted from a circular region with a radius of 20 pixels (1 pixel = $2.36''$), while background events were extracted from a circular region with radius of 50 pixels far away from the source region and from other bright sources. Ancillary response files were generated with `xrtmkarf`, and account for different extraction regions, vignetting and point-spread function corrections. We used the spectral redistribution matrices v013 in the calibration database maintained by HEASARC. Considering the small number of photons collected (< 200 counts) the spectra were rebinned with a minimum of 1 count per bin and we used the Cash statistic (Cash 1979). We fitted the spectrum with an absorbed power law using the photoelectric absorption model `tbabs` (Wilms et al. 2000), with a neutral hydrogen column density fixed to its Galactic value (2.79×10^{21} cm⁻²; Kalberla et al. 2005). The results are reported in Table 5. The observations suggest that TXS 0536+145 was in a relatively bright state on 2012 April 4, after the γ -ray flare, with a flux roughly a factor of 2 higher than during April 18 and November 15. In the past, the source was not detected by the *ROSAT* all-sky survey; thus this is the first detection in X-rays.

During the *Swift* pointing in 2012 April the UVOT instrument observed TXS 0536+145 in all its optical (v , b , and u) and UV ($w1$, $m2$, and $w2$) photometric bands. On 2012 November 15 only observations with the V filter were performed. We analyzed the data using the `uvotsource` task included in the `HEASoft` package. Source counts were extracted from a circular region of $5''$ radius centred on the source, while background counts were derived from a circular region of $10''$ radius in the source neighbourhood. Due to severe Galactic absorption and the short exposures the source was not detected by UVOT in any of the filters. Upper limits are calculated using the UVOT photometric sys-

**Figure 3.** Light curves at 8.4 GHz (*top*), 15 GHz (*middle*) and 24 GHz (*bottom*) of TXS 0536+145. Filled circles are VLBA data, triangles are Medicina data at 8.4 GHz, and crosses are EVN data at 22 GHz.

tem when the analysis provided a detection significance $< 3\sigma$. As a reference on April 4 the lower limits on the magnitudes are: $v > 18.64$, $b > 19.82$, $u > 19.41$, $w1 > 19.22$, $m2 > 19.33$, $w2 > 19.17$.

5 RESULTS

5.1 Flux variability

In 2012 TXS 0536+145 showed strong variability throughout the entire electromagnetic spectrum. The source was not present in the first two *Fermi*-LAT catalogues (Abdo et al. 2010b; Nolan et al. 2012) and no EGRET γ -ray object was reported at the location of the source. However, on 2012 March 22 the source underwent a major γ -ray flare reaching an apparent isotropic luminosity of 6.6×10^{49} erg s⁻¹, which is the second most luminous γ -ray flare from a blazar after 3C 454.3 ($L_{\gamma} \sim 2 \times 10^{50}$ erg s⁻¹, Abdo et al. 2011), and is comparable with those observed in other bright blazars, like PKS 1510–089 ($L_{\gamma} \sim 4 \times 10^{48}$ erg s⁻¹, Orienti et al. 2013), PKS 1830–211 ($L_{\gamma} \sim 3 \times 10^{49}$ erg s⁻¹, Abdo et al., submitted), and PKS 1622–297 ($L_{\gamma} \sim 4 \times 10^{48}$ erg s⁻¹, Mattox et al. 1997).

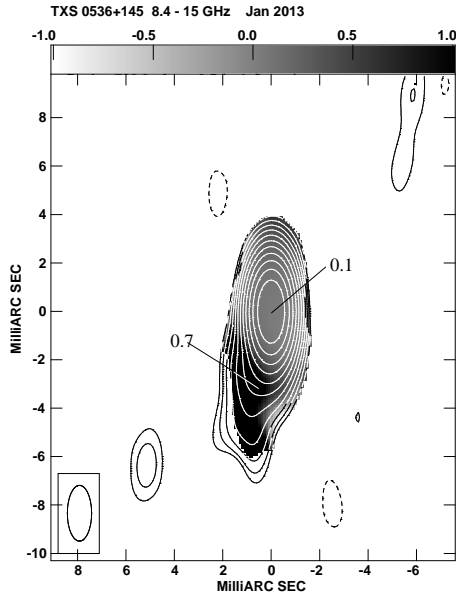


Figure 4. Grey-scale spectral index image between 8.4 and 15 GHz superimposed on the low-resolution 8.4-GHz contours. The peak flux density is 720.9 mJy/beam. The first contour level is 0.5 mJy/beam, which corresponds to three times the noise level measured on the image plane. Contour levels increase by a factor of 2. The restoring beam is plotted on the bottom left corner. The grey-scale is shown by the wedge at the top of the spectral index image.

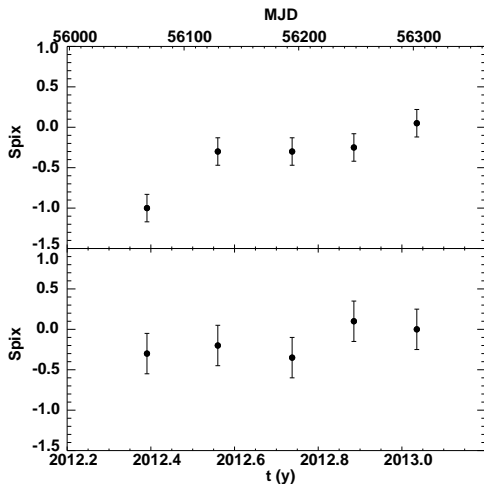


Figure 5. Spectral index computed between 8.4 and 15 GHz (*upper panel*) and between 15 and 24 GHz (*lower panel*) for the five VLBA observing epochs.

Before this flare the source was first detected in γ rays on 2012 January showing an enhancement of its high-energy activity, but without reaching a similar peak flux (Fig. 1). Interestingly, a possible double hump is observed in the radio light curves. From Fig. 3 it seems that the first peak in the 15 GHz light curve occurs at the end of 2012 May, while the second peak is observed at the end of 2012 September, although the time sampling of the observations is not accurate enough to constrain more precisely the peak of the radio outbursts. At 24 GHz the first peak is harder to constrain. At 8.4 GHz the variations are smoother and delayed by ~ 2 months with respect to what is observed at

higher radio frequencies. This agrees with the presence of opacity effects. In both high activity states the increase of the γ -ray emission leads the radio variability at 15 and 24 GHz with a time lag of about 4–5 months.

The aim of the *Swift* observations was to unveil the counterpart of the γ -ray flaring object, and not a detailed study of the optical/X-ray variability. *Swift* observations pointed out that in X-rays the source was in a high activity state after the 2012 March flare, with a flux roughly two times higher than what was observed in the subsequent observing epochs. The high Galactic absorption precluded the detection in the UV bands and in the optical U-band and B-band, and no information about the activity state at such wavelengths could be obtained. The lack of detection in the V band is likely due to the short exposure time of the *Swift* observations. As a comparison, optical observations performed with 70-cm AZT-8 (CrAO, Ukraine)⁵ on 2012 March 26, i.e. a few days after the peak of the γ -ray flare, detected TXS 0536+145 with a magnitude $V=18.7\pm 0.1$ consistent within the uncertainties, with the upper limit estimated by *Swift* observations.

5.2 Spectral variability

TXS 0536+145 hardened its γ -ray spectrum during the flaring episode. In 2012 March, i.e. the month of the highest activity, the photon index was $\Gamma_\gamma = 2.05\pm 0.08$. This value is harder than the mean photon index, $\Gamma_\gamma = 2.37\pm 0.09$ derived between 2011 August and 2013 August. In addition, during the period of highest activity, the spectral shape was better reproduced by a log parabola model instead of a power law, indicating the presence of a significant curvature in the γ -ray spectrum, which was not observed during the average activity state.

No significant change in the photon index is observed in the X-rays.

The radio spectral index analysis is a quite difficult task for VLBI, since it is not possible to obtain a well matched uv -coverage at the various frequencies, particularly at the short spacings. In addition, the opacity of the source slightly changes the position of the core at the various frequencies. With the aim of studying changes in the spectral index distribution, in addition to the full-resolution images, for each observing epoch we produced VLBA low-resolution images at each frequency using the same uv -range (between 17 M λ and 242 M λ), the same image sampling, restoring beam, and natural grid weighting. An example of spectral index image is presented in Fig. 4. Variations in the spectral index computed considering the total flux density between 8.4 and 15 GHz, and between 15 and 24 GHz are reported in Fig. 5. Between 8.4 and 15 GHz the spectrum was inverted after the γ -ray flare, with a spectral index $\alpha_{8.4}^{15} = -1.0 \pm 0.2$, then it flattened to a value $\alpha_{8.4}^{15} = 0.1 \pm 0.2$. At the highest frequencies, the variation of the spectral shape is smoother and the spectral index α_{15}^{24} ranges between -0.3 ± 0.3 and 0.1 ± 0.3 . Errors have been computed assuming the error propagation theory.

⁵ http://lerga.crao.crimea.ua/Instr/azt8_en.html

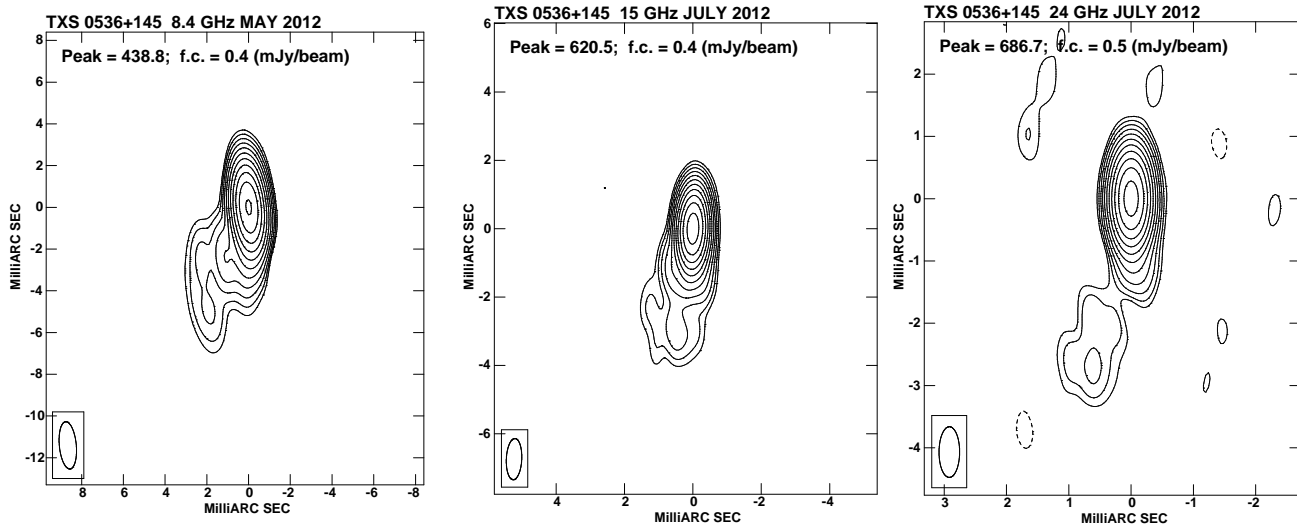


Figure 6. VLBA images of TXS 0536+145 at 8.4 GHz (*left*), 15 GHz (*center*), and 24 GHz (*right*). On each image, we provide the peak flux density in mJy/beam and the first contour (f.c.) intensity in mJy/beam, which corresponds to three times the off-source noise level. Contour levels increase by a factor of 2. The restoring beam is plotted in the bottom-left corner.

5.3 Radio morphology

When observed with parsec-scale resolution the radio source TXS 0536+145 shows a typical core-jet structure (Fig. 6). The radio emission is dominated by the compact bright component, which accounts for about 90 per cent of the total flux density at 8.4 GHz, and about 95 per cent at 15 and 24 GHz. The jet emerges from the main component with a position angle of about 180° , then at ~ 1.5 mas (i.e. ~ 12 pc) it slightly changes orientation to about 160° and extends to ~ 6 mas (i.e. ~ 48 pc). Thanks to the higher angular resolution, the EVN image provides a deeper look into the jet base on sub-milliarcsecond scale (Fig. 7), while lower sensitivity and worse sampling of the short spacing with respect to the VLBA prevent the detection of most of the extended emission from the jet.

No significant changes in the source structure are found by the analysis of the multi-epoch images.

Both the spectral and flux density variability arise from the core component as pinpointed by the multi-epoch high angular resolution images. The jet structure has a steep spectrum, $\alpha_{8.4}^{15} = 0.7 \pm 0.2$, and does not show significant variability.

The similar flux density measured by the Medicina single-dish telescope and the VLBA at 8.4 GHz indicates that no significant emission extending on kpc scale is present.

6 DISCUSSION

The flux increase detected in γ -rays and at lower energies is a strong indication that the flaring γ -ray source is associated with the radio source TXS 0536+145, becoming the γ -ray flaring blazar at the highest redshift observed so far. The radio-to- γ -ray data collected by the multi-band monitoring campaign triggered by the high energy flare allowed us to investigate the physical properties of this

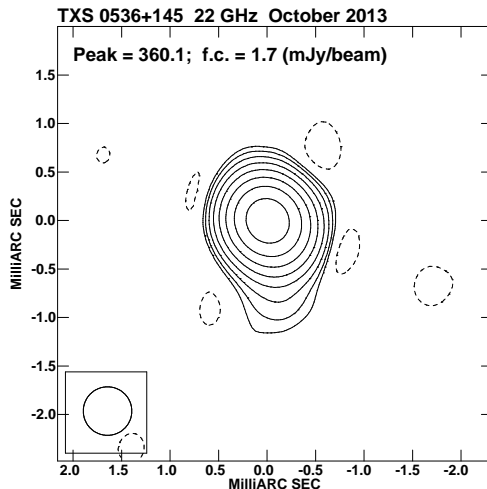


Figure 7. EVN image of TXS 0536+145 at 22 GHz. The image is restored with a circular Gaussian of FWHM = 0.5 mas, plotted on the bottom left corner. On the image we provide the peak flux density in mJy/beam and the first contour (f.c.) intensity in mJy/beam, which corresponds to three times the off-source noise level. Contour levels increase by a factor of 2.

source and to make a comparison with the characteristics of the high redshift population detected in γ -rays so far.

6.1 The high activity state

TXS 0536+146 was in a γ -ray low activity state during the first two years of *Fermi*-LAT observations. In 2012 the source entered in a high activity state: it was detected on a monthly time scale for roughly the whole year (Fig. 1, upper

panel), and on daily time scale in January and March during two major outbursts (Fig. 1, bottom panel). In particular, during the 2012 March flare the source reached an apparent isotropic γ -ray luminosity of about 6.6×10^{49} erg s $^{-1}$, similar to the extreme luminosity reached by the brightest FSRQ like 3C 454.3 and PKS 1510-089 (e.g. Abdo et al. 2011; Orienti et al. 2013).

In the radio band the light curves show a double enhancement which is likely the counterpart at low energies of the two γ -ray outbursts. The time sampling of the radio observations is not adequate for a proper determination of the flaring time. The time lag between the γ -ray flares and the radio counterparts at 15 and 24 GHz is about 4 and 6 months in the observer frame for the first and second outburst respectively, which means a delay of about 1 and 1.5 months in the source frame. This value is consistent with the time-lag of 1.2 months found between γ -ray and radio variability in a few samples of γ -ray emitting blazars (Pushkarev et al. 2010; Fuhrmann et al. 2014).

The observing frequencies 8.4, 15, and 24 GHz correspond to 31, 55, and 88 GHz in the source frame, where the opacity effects should be less severe. In addition, observations at millimeter wavelengths of flaring blazars suggested that the onset of the radio variability seems to lead the γ -ray flare, with a median time delay in the source frame of about one month (Leon-Tavares et al. 2011). The lack of radio observations before the flaring episodes precluded an accurate investigation of the radio light curves at 15 and 24 GHz before those episodes. By contrast, the availability of archival data at 8.4 GHz allowed us to investigate the radio behaviour from 2011 January to September. No evidence of flux density enhancement is found (Table 2). This indicates that the time lag between the beginning of the radio flare and the first γ -ray peak is shorter than 5 months, which corresponds to approximately 1.3 months in the source frame.

Strong γ -ray flares are often found to be associated with the emergence of new superluminal jet components which should be the observational manifestation of the shock propagating along the jet (Jorstad et al. 2001; Orienti et al. 2013; Jorstad et al. 2013). No evidence of a superluminal component is found in TXS 0536+145 by the comparison of the multi-epoch images at 22 GHz. This may be related to the high redshift of the target. We set an upper limit on the apparent separation velocity v_{app} using:

$$v_{\text{app}} = \frac{D_L}{(1+z)} \frac{\theta}{t_{\text{obs}}} \quad (1)$$

where θ is the angular resolution, t_{obs} is the time interval spanned by the EVN observations, D_L is the luminosity distance, and z is the redshift. If in Equation 1 we assume $\theta = 0.5$ mas (i.e. roughly the resolution of the EVN observations) and $t_{\text{obs}} = 500$ days which corresponds to the time interval spanned by the EVN observations, we estimate that the jet component should have $v_{\text{app}} \geq 35c$ to be detected at the resolution of our multi-epoch radio data. Such high apparent velocity is not commonly observed even in the most extreme blazars (Lister et al. 2013, 2009b; Jorstad et al. 2001).

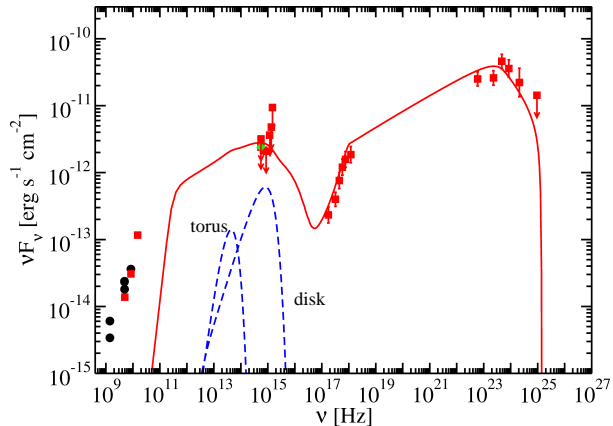


Figure 8. SED data (squares) and model fit (solid curve) of TXS 0536+145 in flaring activity with the model components shown as dashed curves. Filled circles in the radio band are archival radio data, while the filled diamond in the optical regime refers to the detection in V-band on 2012 March 26 by the 70-cm AZT-8 telescope (see Section 5.1).

6.2 SED Modeling

We modeled the SED of TXS 0536+145 with a combination of synchrotron, synchrotron self-Compton (SSC), and external Compton (EC) non-thermal emission. We also included thermal emission by an accretion disc and dust torus. The modeling details can be found in Finke et al. (2008) and Dermer et al. (2009). The synchrotron component considered in the model is self-absorbed below 10^{11} Hz and the radio data were not fitted in the model.

The black hole mass for this object is not constrained, so we assumed its mass to be $M_{\text{BH}} = 10^9 M_{\odot}$. Unfortunately, unlike the case of the high-redshift blazar S5 0014+813 (Ghisellini et al. 2009a) we are not able to estimate the accretion disc parameters from the optical data, since the optical data for TXS 0536+145 are upper limits with the exception of a single detection in the V-band (see Section 5.1). With these data we can only put an upper limit on the disc luminosity of about 10^{47} erg s $^{-1}$, slightly below the Eddington limit for a $10^9 M_{\odot}$ black hole, and we modelled the source in a sub-Eddington accretion regime. We used a variability timescale of 1 day to constrain the size of the emitting region, consistent with the source's γ -ray light curve. The results of the modeling can be found in Table 6 and Figure 8 (see Dermer et al. 2009, for a description of the model parameters). The model has the magnetic field in equipartition, which means that the energy stored in relativistic particles is approximately equal to the magnetic energy. The EC seed photon source was chosen to be those from the dust torus, and this external radiation field was treated as an isotropic, monochromatic photon source. The dust torus parameters were chosen to be consistent with the relation between inner radius, disc luminosity, and dust temperature from Nenkova et al. (2008). Due to the rather poor optical coverage, the model parameters are not well constrained.

Table 6. Model parameters.

Parameter	Symbol	Value
Redshift	z	2.69
Bulk Lorentz Factor	Γ	30
Doppler factor	δ_D	30
Magnetic Field [G]	B	1.2
Variability Timescale [s]	t_v	8.64×10^4
Comoving radius of blob [cm]	R'_b	2.1×10^{16}
Low-Energy Electron Spectral Index	p_1	2.5
High-Energy Electron Spectral Index	p_2	3.5
Minimum Electron Lorentz Factor	γ'_{\min}	3.0
Break Electron Lorentz Factor	γ'_{brk}	2.6×10^3
Maximum Electron Lorentz Factor	γ'_{\max}	2.0×10^4
Black hole Mass [M_\odot]	M_{BH}	1.0×10^9
Disc luminosity [erg s^{-1}]	L_{disc}	3.9×10^{46}
Inner disc radius [R_g]	R_{in}	6.0
Seed photon source energy density [erg cm^{-3}]	u_{seed}	1.3×10^{-3}
Seed photon source photon energy	ϵ_{seed}	1.0×10^{-6}
Dust Torus luminosity [erg s^{-1}]	L_{dust}	1.1×10^{46}
Dust Torus radius [cm]	R_{dust}	1.0×10^{19}
Dust temperature [K]	T_{dust}	2000
Jet Power in Magnetic Field [erg s^{-1}]	$P_{j,B}$	4.3×10^{45}
Jet Power in Electrons [erg s^{-1}]	$P_{j,e}$	9.8×10^{45}

6.3 The high-redshift γ -ray population

To have a full characterization of the physical properties of TXS 0536+145, we compare its observational characteristics with those shown by the population of high redshift ($z > 2$) γ -ray sources. To this purpose we selected the γ -ray sources from the 2LAC that are associated at high confidence with a blazar at redshift $z > 2$ (Ackermann et al. 2011). Sources with multiple associations were discarded. The final sample of high-redshift γ -ray sources consists of 35 FSRQ.

Fig. 9 shows the photon index versus the redshift for the high-redshift sample. The photon index ranges between 1.6 and 3.0, with a distribution mean value $\Gamma_\gamma = 2.4 \pm 0.3$, which is in agreement with the mean value $\Gamma_\gamma = 2.42 \pm 0.17$ derived for the whole FSRQ population from 2LAC (Ackermann et al. 2011). The photon index of TXS 0536+145 is $\Gamma_\gamma \sim 2.4$, in excellent agreement with the mean value, and it gets harder during the flare ($\Gamma_\gamma \sim 2.0$). Among the high-redshift γ -ray sources, changes of the photon index during different activity states were investigated for the source 4C +71.07 (alias S5 0836+71) by Akyuz et al. (2013). This source has a redshift $z = 2.218$ and its photon index varies between 2.95 and 2.65 during the low activity and flaring states, indicating a softer spectrum than that observed in TXS 0536+145. It is worth noting that during the flaring state the spectrum of both sources deviates from a power law, showing a significant curvature and a log-parabola shape.

New γ -ray flaring objects at high redshift are not commonly detected. So far 10 sources with $z > 2$ have been observed during a γ -ray flare, and only TXS 0536+145 is not part of the 2LAC.

Fig. 10 plots the γ -ray luminosity ($E > 100$ MeV) versus redshift, for high-redshift γ -ray sources in the 2LAC. The

γ -ray luminosity, L_γ is computed following Ghisellini et al. (2009b):

$$L_\gamma = 4\pi D_L^2 \frac{S_\gamma}{(1+z)^{2-\Gamma_\gamma}} \quad (2)$$

where S_γ is the energy flux between 100 MeV and 100 GeV, and Γ_γ is the photon index. For the 2LAC sources, we calculated the γ -ray luminosity considering in Eq. 2 the energy flux reported in the 2FGL (Nolan et al. 2012). The γ -ray luminosity ranges between 2.5×10^{46} erg s^{-1} and 2×10^{48} erg s^{-1} , with a median value $L_\gamma \sim 1.6 \times 10^{47}$ erg s^{-1} . As was already pointed out in Ackermann et al. (2011), high-redshift objects tend to be the most luminous ones due to the observational sensitivity limitation. In Fig. 10 we report the luminosity of both TXS 0536+145 and 4C +71.07 during the flare and the average state. In addition, for TXS 0536+145 we report the upper limit computed by considering the first two years of *Fermi*-LAT observations, i.e. when the source was not detected. The upper limit, $L_\gamma < 2.3 \times 10^{47}$ erg s^{-1} , is consistent with the luminosity values of the other high-redshift blazars.

During the flare, TXS 0536+145 increased its γ -ray luminosity more than an order of magnitude with respect to the average luminosity, reaching $L_\gamma = 6.6 \times 10^{49}$ erg s^{-1} . Such a huge increase of the γ -ray luminosity was observed from 3C 454.3 during the exceptional flare that occurred in 2010 November. The peak luminosity $L_\gamma \sim 2 \times 10^{50}$ erg s^{-1} was more than an order of magnitude higher than the average luminosity $L_\gamma \sim 5 \times 10^{48}$ erg s^{-1} from the 2FGL (Nolan et al. 2012).

To investigate a change in the spectrum during the high activity period, in Fig. 11 we plot the photon index versus the γ -ray luminosity. It is clear that both TXS 0536+145 and 4C +71.07 show a “harder when brighter” effect, in agreement with what was found for other variable blazars

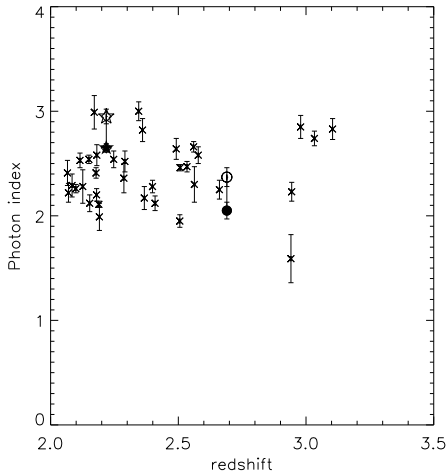


Figure 9. Photon index versus redshift. Crosses are the high redshift sources from the 2LAC with $z > 2$ (Ackermann et al. 2011), the empty and filled circles are TXS 0536+145 during the average activity between 2011 August and 2013 August, and during the flare (2012 March), respectively. Empty and filled stars refer to the high redshift flaring object 4C+71.07 during the low activity state and the high activity state, respectively (Akyuz et al. 2013).

(Abdo et al. 2010a). The hardening of the spectrum during a flare from a FSRQ should allow us to detect photons at higher energies than those observed during an average state. Considering the EBL model discussed in Finke et al. (2010), at the redshift of TXS 0536+145 the optical depth should be $\tau \sim 1$ for 40 GeV photons. The maximum photon energy observed from TXS 0536+145 is 11.2 GeV and is consistent with the current EBL models.

7 CONCLUSIONS

In this paper we presented the results of the multi-wavelength campaign for the flaring blazar TXS 0536+145 carried out after two flaring γ -ray events in 2012 January and March. This source was not part of the 1FGL and 2FGL catalogues, indicating its low γ -ray activity state during the first two years of *Fermi*-LAT observations. During the brightest γ -ray flare the source reached an apparent isotropic γ -ray luminosity of 6.6×10^{49} erg s $^{-1}$, comparable to the values achieved by the most luminous and variable blazars. This episode triggered a monitoring campaign from radio to X-rays performed by VLBA, EVN, Medicina, and *Swift*. The spatial association between the γ -ray source and the low energy counterpart, together with the detection of multi-wavelength variability allowed us to firmly identify the γ -ray object with TXS 0536+145, becoming the highest redshift γ -ray flaring source detected so far.

The analysis of the γ -ray *Fermi*-LAT light curve pointed out that the source was first detected in a high activity state in 2012 January, without reaching the peak luminosity observed during the following flare. A similar variability is observed in the radio band, where a possible double hump is seen in the light curves at 15 and 24 GHz. However, the variability at the two extremes of the electromagnetic

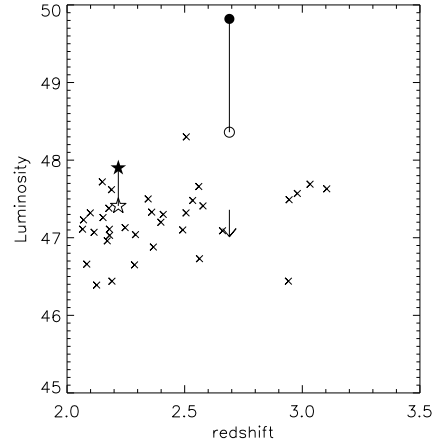


Figure 10. Luminosity versus redshift. Crosses are the high redshift sources from the 2LAC with $z > 2$ (Ackermann et al. 2011), the empty and filled circles are TXS 0536+145 during the average activity between 2011 August and 2013 August, and during the flare (2012 March), respectively. The arrow is the luminosity upper limit for TXS 0536+145 computed during the low activity state. Empty and filled stars refer to the high redshift flaring object 4C+71.07 during the low activity state and during the flare, respectively (Akyuz et al. 2013).

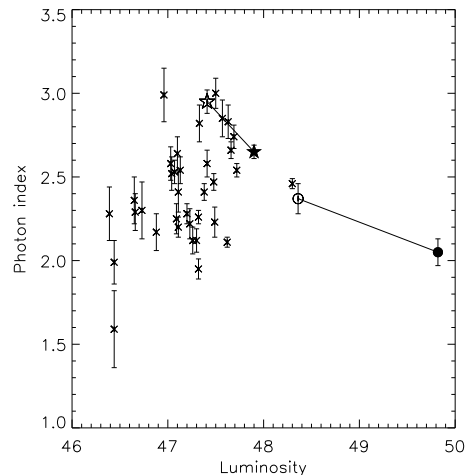


Figure 11. Photon index versus luminosity. Crosses are the high redshift sources from the 2LAC with $z > 2$ (Ackermann et al. 2011), the empty and filled circles are TXS 0536+145 during the average activity between 2011 August and 2013 August, and during the flare (2012 March), respectively. Empty and filled stars refer to the high redshift flaring object 4C+71.07 during the low activity state and the flaring state, respectively (Akyuz et al. 2013).

spectrum seems delayed and the γ -ray leads the radio with a time lag of about 4-6 months, which corresponds to about 1.5 months in the source frame.

In the VLBI radio images this source displays a core-jet structure on the pc scale. Both the flux density and spectral variability are from the core component, while the jet does not show any significant change. The delay between the γ -ray and radio variability and its location in the unresolved

central radio component indicates that the γ -ray flare is produced in the innermost region of the AGN close to the supermassive black hole, where the opacity severely affects the radio emission. As the relativistic plasma expands, its emission becomes optically thin at long wavelengths and the variability is observed in the radio band.

No evidence of a newly ejected superluminal component is found during the 16 months spanned by the VLBI monitoring campaign.

The broad-band SED is well fitted by a synchrotron/external Compton model where the seed photons may be those from the dust torus. In the γ -rays the spectrum becomes harder during the flare, and deviates from a simple power law, showing a curvature that was not observed in the average activity state. Despite the harder spectrum, no significant emission above 10 GeV is observed. The EBL should cause an energy-dependent suppression of the γ -ray flux from blazars that increases for larger redshifts. Such effect was observed in a sample of BL Lac object with redshift up to $z \sim 1.6$ (Ackermann et al. 2012). At the redshift of TXS0536+145 the flux attenuation should be observable below 10 GeV, leading to a curvature of the spectrum. A significant spectral curvature was observed during the 2012 March γ -ray flare, but the statistics are not enough for testing if it is related to the EBL attenuation, to the Klein-Nishina effect, or if it is intrinsic to the spectrum of the source. The improved sensitivity of the LAT at a few GeV with Pass 8 data will be important for characterizing in more detail the γ -ray spectrum of this high-redshift blazar.

ACKNOWLEDGMENTS

We thank D. Blinov for providing the 70-cm AZT-8 optical data. We are grateful to D.J. Thompson and S. Digel for carefully reading the manuscript. We thank the anonymous referee for useful suggestions. The VLBA is operated by the US National Radio Astronomy Observatory which is a facility of the National Science Foundation operated under a cooperative agreement by Associated Universities, Inc. The European VLBI Network is a joint facility of European, Chinese, South African and other radio astronomy institutes funded by their national research councils. The research leading to these results has received funding from the European Commission Seventh Framework Programme (FP/2007-2013) under grant agreement No. 283393 (RadioNet3).

The *Fermi* LAT Collaboration acknowledges generous ongoing support from a number of agencies and institutes that have supported both the development and the operation of the LAT as well as scientific data analysis. These include the National Aeronautics and Space Administration and the Department of Energy in the United States, the Commissariat à l’Energie Atomique and the Centre National de la Recherche Scientifique / Institut National de Physique Nucléaire et de Physique des Particules in France, the Agenzia Spaziale Italiana and the Istituto Nazionale di Fisica Nucleare in Italy, the Ministry of Education, Culture, Sports, Science and Technology (MEXT), High Energy Accelerator Research Organization (KEK) and Japan Aerospace Explo-

ration Agency (JAXA) in Japan, and the K. A. Wallenberg Foundation, the Swedish Research Council and the Swedish National Space Board in Sweden. Additional support for science analysis during the operations phase is gratefully acknowledged from the Istituto Nazionale di Astrofisica in Italy and the Centre National d’Études Spatiales in France. This research has made use of the data from the MOJAVE database that is maintained by the MOJAVE team (Lister et al. 2009, AJ, 137, 3718). Part of the research is based on observations with the Medicina telescope operated by INAF - Istituto di Radioastronomia. We acknowledge the Enhancement Single-Dish Control System (ESCS) Development Team at the Medicina telescope.

This research has made use of the NASA/IPAC Extragalactic Database NED which is operated by the JPL, Californian Institute of Technology, under contract with the National Aeronautics and Space Administration.

REFERENCES

- Abdo, A.A., et al. 2010a, ApJ, 710, 1271
 Abdo, A.A., et al. 2010b, ApJS, 188, 405
 Abdo, A.A., et al. 2011, ApJ, 733, L26
 Ackermann, M., et al. 2011, ApJ, 743, 171
 Ackermann, M., et al. 2012, Science, 338, 1190
 Ackermann, M., et al. 2013, ApJS, 209, 34
 Ajello, M., Alexander, D.M., Greiner, J., Madejski, G.M., Gehrels, N., Burlon, D. 2012, ApJ, 749, 21
 Akyuz, A., et al. 2013, A&A, 556, 71
 Atwood, W. B., et al. 2009, ApJ, 697, 1071
 Barthelmy, S. D., et al. 2005, SSRv, 120, 143
 Baumgartner, W. H., et al. 2013, ApJS, 207, 19
 Burrows, D. N., et al. 2005, SSRv, 120,165
 Cash, W. 1979, ApJ, 228, 939
 Dermer, C.D., Finke, J.D., Krug, H., Böttcher, M. 2009, ApJ, 692, 32
 Finke, J.D., Dermer, C.D., Böttcher, M. 2008, ApJ, 686, 181
 Finke, J.D., Razzaque, S., Dermer, C.D. 2010, ApJ, 712, 238
 Franceschini, A., Rodighiero, G., Vaccari, M. 2008, A&A, 487, 837
 Fuhrmann, L., et al. 2014, MNRAS, 441, 1899
 Gehrels, N., et al. 2004, ApJ, 611, 1005
 Ghisellini, G., Foschini, L., Volonteri, M., Ghirlanda, G., Haardt, F., Burlon, D., Tavecchio, F. 2009a, MNRAS, 399, 24
 Ghisellini, G., Maraschi, L., Tavecchio, F. 2009b, MNRAS, 396, 105
 Gould, R.J., Schreder, G. 1967, Phys. Rev. Lett. 16, 252
 Jorstad, S., Marscher, A.P., Mattox, J.R., Wehrle, A.E.; Bloom, S.D.; Yurchenko, A.V. 2001, ApJS, 134, 181
 Jorstad, S.G., et al. 2013, ApJ, 773, 147
 Kalberla, P. M. W., et al.2005, A&A, 440, 775
 Leon-Tavares, J., Valtaoja, E., Tornikoski, M., Lähteenmäki, A., Nieppola, E. 2011, A&A, 532, 146
 Lister, M.L., et al. 2009a, AJ, 137, 3718
 Lister, M.L., et al. 2009b, AJ, 138, 1874
 Lister, M.L., et al. 2013, AJ, 146, 120
 Mattox, J. R., et al. 1996, ApJ, 461, 396
 Mattox, J.R., Wagner, S.J., Malkan, M., McGlynn, T.A.,

- Schachter, J.F., Grove, G.E., Johnson, W.N., Kurfess, J.D. 1997, ApJ, 476, 692
- Nenkova, M., Sirocky, M. M., Nikutta, R., Ivezić, Ž., Elitzur, M. 2008, ApJ, 685, 160
- Nolan, P., et al. 2012, ApJS, 199, 31
- Orienti, M., D'Ammando F. 2012, ATel, 3999
- Orienti, M., et al. 2013, MNRAS, 428, 2418
- Pushkarev, A.B., Kovalev, Y.Y., Lister, M. 2010, ApJL, 722, 7
- Roming, P. W. A., et al. 2005, SSRv, 120, 95
- Sowards-Emmerd, D., Romani, R.W., Michelson, P.F., Healey, S.E., Nolan, P.L. 2005, ApJ, 626, 95
- Wilms, J., et al. 2000, ApJ, 542, 914